A FIRST REPORT ON DEFORMATION-MECHANISM MAPS*

M. F. ASHBY†

This report introduces the idea of *deformation–mechanism maps*: maps which display the fields of stress and temperature in which a particular mechanism of plastic flow is dominant. Most materials have the capacity to deform by several alternative and independent mechanisms: dislocation glide, diffusional flow and dislocation creep are examples. Each appears on the map as a field. A point on a map then identifies the dominant mechanism and indicates the resulting strain-rate.

Three applications of the maps are discussed. First, they permit a study of the effect of crystal structure and atomic bonding on plastic flow. Second, they help in the design of experiments to study a given flow mechanism and in locating, identifying and characterizing missing mechanisms. And, third, they are useful in a qualitative way for choosing a material for engineering applications, for predicting the mechanism by which it deforms and hence in selecting, or predicting the effects, of strengthening mechanisms.

CARTES DES MECANISMES DE DEFORMATION

L'auteur introduit l'idée des cartes des mécanismes de déformation: cartes qui donnent les champs de contraintes et de températures dans lesquels un mécanisme plastique particulier est dominant. La plupart des matériaux sont capables de se déformer par différents mécanismes possibles et indépendants: le glissement des dislocations, le fluage des dislocations ou par diffusion, en sont des exemples. Chacun d'eux apparaît sur la carte comme un champ. Un point sur une carte identifie donc le mécanisme dominant et indique la vitesse de déformation résultante.

L'auteur présente trois applications de ces cartes. Elles permettent d'abord une étude de l'influence de la structure du cristal et des liaisons atomiques sur la plasticité. Deuxièmement, elles aident à choisir les expériences nécessaires pour étudier un mécanisme donné, et à localiser, identifier et caractériser les mécanismes manquants. Troisiémement, elle sont utiles qualitativement pour le choix des matériaux à applications industrielles, pour la prévision des mécanismes par lesquels ils se déforment et, à partir de là, pour sélectionner ou prévoir les effets des mécanismes de consolidation.

EIN ERSTER BERICHT ÜBER EINE DARSTELLUNG DER VERFORMUNGS-MECHANISMEN IN EINER ART LANDKARTE

In diesem Bericht wird die Idee von Übersichtskarten oder Landkarten der Verformungsmechanismen vorgestellt: Die Landkarten zeigen Spannungs- und Temperaturfelder, in denen bestimmte Mechanismen des plastischen Fließens dominieren. In den meisten Materialien können mehrere alternative und unabhängige Verformungsmechanismen wirksam sein: Versetzungsgleiten, Fließen aufgrund von Diffusionsvorgängen und Versetzungskriechen seien als Beispiele genannt. Jeder Mechanismus erscheint auf der Landkarte als ein Feld. Ein Punkt auf der Landkarte gibt dann sofort den dominierenden Mechanismus und einen Hinweis auf die Abgleitgeschwindigkeit.

Drei Anwendungen der Landkarten werden diskutiert. Erstens erlauben sie die Untersuchung des Einflusses der Kristallstruktur und der chemischen Bindung auf das plastische Fließen. Zweitens helfen sie beim Entwurf von Experimenten zur Untersuchung eines bestimmten Fließmechanismus sowie beim Auffinden, bei der Identifizierung und Charakterisierung fehlender Mechanismen. Drittens sind sie sehr nützlich bei der Wahl von Materialien für Anwendungszwecke, bei der Vorhersage des Mechanismus, durch den sich das Material verformt und somit bei der Auswahl und Vorhersage der Einflüsse von Verfestigungsmechanismen.

1. INTRODUCTION: DEFORMATION MECHANISM MAPS

When crystalline matter is plastically deformed, its crystallinity is preserved. There are at least six *distinguishable and independent* ways in which a polycrystal can be deformed and yet remain crystalline. All but one of them involve the motion through the grains, or round their boundaries, of lattice defects.

First, a stress which exceeds the *theoretical shear strength* causes flow even in a defect-free crystal; we call this *defect-less flow* to distinguish it from all other kinds of plastic deformation, since they require defects to be present. Second, the *glide motion of dislocations* can lead to extensive plastic flow. At high temperatures the ability of dislocations to climb as well as glide introduces a third mechanism: *dislocation creep*.‡ Point defects also permit plastic flow when they move: two independent kinds of *diffusional flow* result from flow of point defects through grains and round their boundaries; these fourth and fifth mechanisms are sometimes called Nabarro–Herring creep and Coble creep, respectively. Finally *twinning* provides a sixth mechanism; unlike the others it can supply only a limited amount of deformation.

The aim here is to present in a simple manner the way in which the alternative deformation mechanisms compete; that is, the values of stress and temperature

* Received January 3, 1972.

† Harvard University, Division of Engineering and Applied Physics, Cambridge, Massachusetts 02138.

‡ It may be questioned that dislocation glide and dislocation creep are distinguishable, independent, mechanisms. The two display different and characteristic, activation energies; and give strain-rates which depends on stress in different and characteristic ways. So they are certainly distinguishable mechanisms, both potentially able to permit steady-state deformation. But it is not clear that they are independent. Only alternative, independent mechanisms (i.e. those giving additive strain rates) appear as separate fields. For the purposes of this report we shall treat them as such.

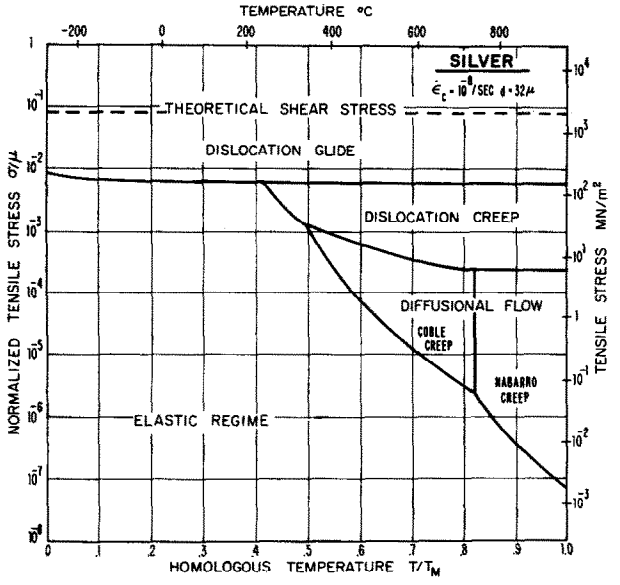

FIG. 1. A deformation–mechanism map for pure silver, of grain size 32 μ, and for a critical strain rate $\dot{\epsilon}_c$ of 10^{-8}/sec.

for which each controls the flow stress. This we do by plotting maps in stress/temperature space.* The space is divided into fields. Within a field, one mechanism is dominant; that is, it supplies a greater strain-rate than any other mechanism. Figure 1 shows one way in which the result can be presented; it is a map for silver. Where the strain-rate is too small to be measurable, an elastic field appears. Throughout we consider steady-state flow only, and we assume that fracture does not intervene.

We now discuss the constitutive equations used to construct the maps. I have attempted to choose the form which, in my judgement, best combines simplicity with a uniform level of accuracy. Exhaustive references to the historical development of these equations and discussions of their reliability would be out of place; instead I simply refer in each case to recent reviews.

2. CONSTITUTIVE EQUATIONS

Standard relations between tensile stress and tensile strain rate are used to construct the maps. They, and the mechanisms on which they are based, are outlined briefly below. We treat all the mechanisms as capable of permitting *steady-state* flow.

2.1 *Defect-less flow*

A defect-free crystal can, of course, deform plastically. At a sufficiently high stress, planes of atoms in the crystal can be lifted bodily over neighboring planes, producing permanent deformation. The very large stress required to do this has been recalculated and refined repeatedly over the last 40 yr (see Kelly[1]). This *theoretical shear strength* is always of order $\mu/20$ (where μ is the shear modulus) and is practically independent of temperature. Accordingly, we adopt the following simplified constitutive relation to define the defect-less flow field:

$$\left.\begin{aligned} \dot{\epsilon}_1 &= \infty \qquad \frac{\sigma}{\mu} \geq \frac{\sigma^{TH}}{\mu} \\ \dot{\epsilon}_1 &= 0 \qquad \frac{\sigma}{\mu} < \frac{\sigma^{TH}}{\mu} \end{aligned}\right\} \tag{1}$$

where $\dot{\epsilon}$ is the tensile strain-rate and σ^{TH} the tensile stress corresponding to the theoretical shear strength. (Throughout this article, we relate tensile stresses to shear stresses by using the von Mises criterion, yielding $\sigma = \sqrt{3}\tau$, where τ is a shear stress.)

2.2 *Dislocation glide*

Practically all crystals contain dislocations. The great ease with which they move in f.c.c. and h.c.p. crystals means that, in practice, dislocation glide in these crystals is limited by the presence of obstacles to slip: impurities, solute, other dislocations or precipitates. For such crystals, the flow stress is proportional to $\mu b/l$, where l is the obstacle spacing and b the Burger's vector. The constant of proportionality is complicated; it depends on the strength of the obstacles and on the statistics of their distribution. For the purposes of this article we adopt the following constitutive equation for dislocation glide;[2,3]

$$\left.\begin{aligned} \dot{\epsilon}_2 &= \dot{\epsilon}_0 \exp - \frac{\{S - \sigma\}}{kT} ba \qquad \frac{\sigma}{\mu} \geq \frac{\sigma_0}{\mu} \\ \dot{\epsilon}_2 &= 0 \qquad\qquad\qquad\qquad\quad \frac{\sigma}{\mu} < \frac{\sigma_0}{\mu} \end{aligned}\right\} \tag{2a}$$

Here $S = \mu b/l$ describes the flow stress at absolute zero; k is Boltzmann's constant, T the absolute temperature, a the activation area and σ_0 is a cut-off stress, sometimes called the "athermal part of flow stress". $\dot{\epsilon}_0$, the preexponential term, is the strain-rate when $\sigma = S$.

Dislocation motion in b.c.c. and diamond cubic crystals, and in oxides and carbides, is more difficult: the crystal lattice itself resists the motion, in a way which increases rapidly with decreasing temperature. Following Guyot and Dorn[4] I have adopted for this lattice resistance a Peierls potential of parabolic form, such that the activation energy required to move a

* Such a diagram, in approximate form, has been presented by Weertman.[7]

dislocation has the form

$$u = 2u_k \left\{1 - \frac{\sigma_p}{\sigma}\right\}^2$$

Here σ_p is the flow stress at 0°K and u_k the energy of formation of a kink pair. The strain-rate is given by $\dot{\varepsilon}_2'$, where

$$\dot{\varepsilon}_2' = \dot{\varepsilon}_0' \exp - \frac{u}{kT} \qquad (2b)$$

and ε_0' is an appropriate pre-exponential term. Unlike every other constitutive equation discussed in this article, this one does not represent an alternative, independent mechanism. The lattice resistance is a strengthening mechanism, not a deformation mechanism. It must be included by superimposing stresses, not strain rates. In computing the maps, I have assumed that it adds *linearly* to the effect of obstacles. (The superposition of strengthening mechanisms is rarely this simple; see reviews 2 and 3.)

2.3 *Diffusional creep*

Diffusional flow of single ions, either by bulk transport or by grain-boundary transport, leads to the Newtonian-viscous creep of a polycrystal. The two alternative flow paths represent independent, additive contributions to the overall strain-rate. The most recent re-analysis of this problem yields the following combined constitutive equation[5]

$$\dot{\varepsilon}_{3,4} = 14 \frac{\sigma\Omega}{kT} \frac{1}{d^2} D_v \left\{1 + \frac{\pi\delta}{d} \frac{D_B}{D_v}\right\} \qquad (3, 4)$$

relating the tensile strain-rate to the tensile stress. Here Ω is the atomic volume, d the grain size, D_v the bulk self-diffusion coefficient, D_B that for boundary diffusion and δ the effective cross section of a boundary for diffusional transport. When bulk diffusion dominates, the creep is often called *Nabarro–Herring*, or simply *Nabarro-creep*; when, instead, boundary diffusion dominates, it is known as *Coble-creep*. Although a proper treatment yields the combined equation (3, 4), the two processes *are* independent and distinguishable and therefore each qualifies for a field.

2.4 *Dislocation-creep*

At temperatures above about $0.5T_M$, and relatively high stresses, dislocations move through the grains of a polycrystal and aggregate to form cells. The ensuing deformation is apparently diffusion controlled (unlike dislocation glide), but the strain-rate is a non-linear function of stress (unlike diffusional creep). This *dislocation creep* is found experimentally to obey the constitutive relation,[6,7]

$$\dot{\varepsilon}_5 = A \frac{D_v \mu b}{kT} \left(\frac{\sigma}{\mu}\right)^n \qquad (5)$$

where A and n are constants. Although the general form of this equation can be arrived at theoretically (for instance, by postulating that it is simply *diffusional flow* with the grain size replaced by a stress-dependent cell size), no really convincing theory can be said to exist. But it is extraordinarily well documented from an experimental point of view: data exist for the constants A and n for a wide variety of materials.

2.5 *Other mechanisms*

Although it cannot lead to unlimited deformation, twinning is a way of deforming a crystal, while retaining its crystallinity. For f.c.c. metals a twinning field appears at low temperatures; it typically exists only below about 20°K. For hexagonal metals it may extend above room temperature. It has been ignored in the maps shown here.

Other, as yet unidentified (or, at best, speculative) mechanisms certainly exist; we return to this point in Section 4.2. But for the purposes of this report, we shall limit the discussion to the six mechanisms listed above.

3. DEFORMATION-MECHANISM MAPS

3.1 *Construction of the maps*

Consider a two dimensionsl stress/temperature space. As a stress coordinate we use *a normalized tensile* stress σ/μ, where μ is the shear modulus. As temperature coordinate we use *homologous temperature*, T/T_M, where T_M is the melting point of the material. (This normalization has the great advantage of reducing the maps for materials of the same crystal class, and with similar bonding, to a single group.) Let σ/μ range from 10^{-8} to 1, and T/T_M range from 0 to 1; these ranges cover all possible values of the variables ever found in practice.

The construction of the maps involves two stages. We first ask: *in what field of stress/temperature space is a single mechanism dominant*—that is, where does it supply a greater strain-rate than any other single mechanism? The *boundaries of the fields* are obtained by equating pairs of the constitutive equations (1)–(5), and solving for stress as a function of temperature. At a field boundary, the two mechanisms which meet there contribute equally to the strain-rate. At a point where three fields meet, three mechanisms contribute equally. Figure 2 shows the fields obtained in this way.

Any pair of values of stress and temperature now locates a point in a field. From the map we can read-off the dominant mechanism. From the appropriate constitutive equation we can calculate the strain-rate. This allows us to plot *contours of constant strain-rate*

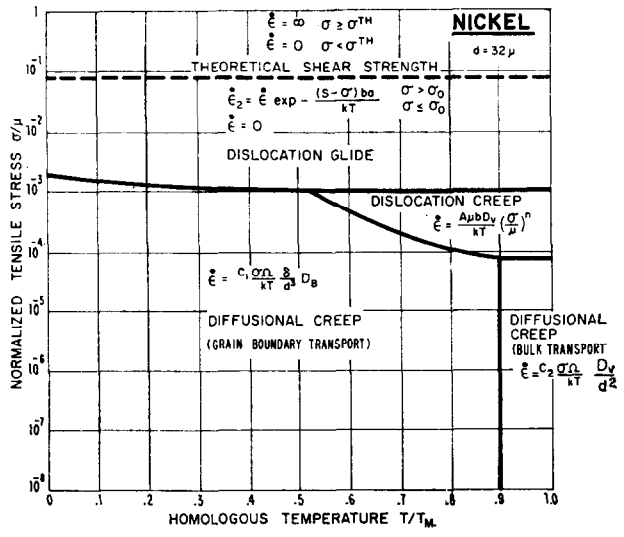

FIG. 2. Mechanism fields for pure nickel with a grain size of 32 μ. The fields are labeled with the appropriate constitutive equation. Field boundaries are obtained by equating constitutive equations.

onto the diagram. Figure 2, modified in this way, is shown in Fig. 3. A second example, for tungsten, is shown in Fig. 4. Details of the calculation appear in the Appendix, together with the very considerable amount of data required for their construction.

We now have a map which is really useful. Knowledge of any pair of the three variables of strain-rate, stress and temperature locates a point on the map, identifies the dominant mechanism or mechanisms, and gives the value of the third variable. Some uses of the maps are discussed in Section 4.

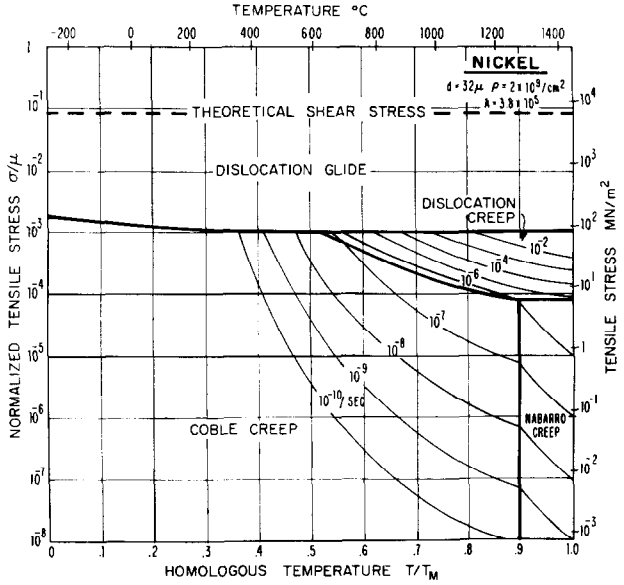

FIG. 3. A complete map for pure nickel with a grain size of 32 μ.

3.2 *Characteristics of the fields*

Each field has its own characteristics. Diffusional creep is strongly grain-size dependent: the others are not. Glide and dislocation creep cause a texture to develop; diffusional creep does not. Diffusional creep is a linear-viscous process; all the others are non-linear. These and other characteristics such as the activation energy, the presence or absence of a transient, etc., help to identify a field.

3.3 *Effect of microstructure*

Consider a map on which one strain-rate contour—that for $\dot{\varepsilon} = 10^{-8}$/sec, appears. We may imagine that our test machine can detect no strain-rate smaller than this. A large field of the map then corresponds to purely elastic (or anelastic) deformation, as shown in Fig. 1.

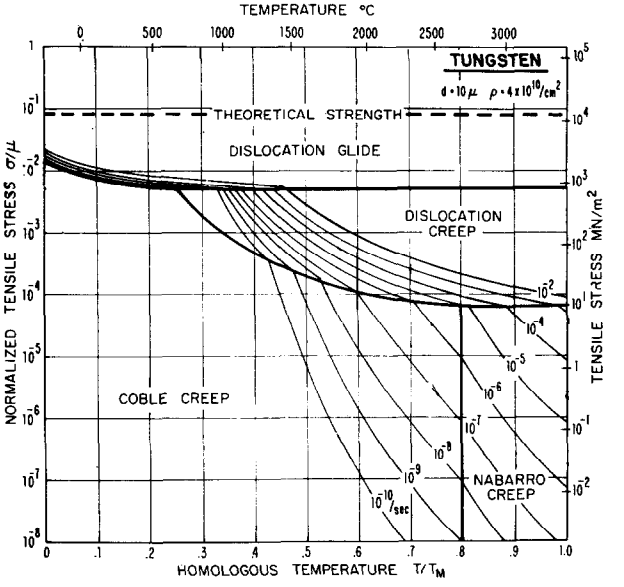

FIG. 4. A complete map for pure tungsten with a grain size of 10 μ.

Figures 5 and 6 show the effect of microstructure on such a map. If the spacing of strong obstacle (l) or the equivalent density of forest dislocations (ρ) is changed, the glide field grows or shrinks as shown crudely in Fig. 5. Strong, *stable*, obstacles also alter the dislocation creep field, but (except under special circumstances) have practically no effect on diffusional creep.

Grain size has a profound effect on diffusional creep (Fig. 6). Decreasing the grain size has a small effect on the glide field, causing a slight strengthening not shown on the figure.

Obviously, microstructure has a profound effect on plastic deformation. At low temperatures, the yield strength is proportional, roughly, to the reciprocal of

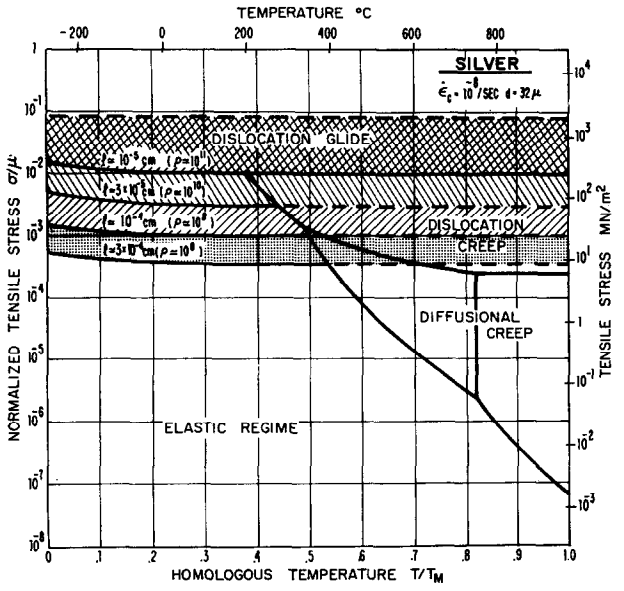

FIG. 5. Changing the obstacle spacing, l, or (equivalently) the dislocation density, ρ, causes the glide field to shrink or expand.

the spacing of obstacles. The high temperature diffusional-creep strength is proportional to the square or the cube of the grain size. These are rapid dependencies, and lead to wide changes of property with microstructures. Note, particularly, that a microstructural change (or a strengthening mechanism) does not affect all fields equally. Point obstacles, for instance, act as a strengthening mechanism for dislocation glide, but do not always inhibit diffusional flow. It does not make sense to precipitation-harden an alloy which (in its use) deforms by diffusional creep.

3.4 *Limitations and extensions of the maps*

The most obvious limitation of the maps in their present form is their limitation to *steady state flow*. Time, or strain-dependent effects are not included. One could construct maps using time or strain-dependent constitutive equations, though displaying the results in a useful way presents problems. A map then represents flow at a given time or strain.

Although the maps shown here are based on *tensile* stress and strain rates, their use is not limited to the tensile stress-state. The stress axis of the diagrams can be regarded as an *equivalent stress*, related to the multiaxial state of stress in a body by the von Mises criterion. The contours of constant strain-rate then become contours of *equivalent strain-rate*, related by an analogous criterion to the strain-rate tensor (see Ref. 8).

Finally, I believe that several mechanisms fields are missing from the present maps. We return to this point later in the report. Even the construction of those which do appear involves approximations, and is, in a number of ways, inadequate (see the Appendix). In certain ways they could be improved; but the major inadequacies reflect a more fundamental problem: the poor level of our understanding of creep, particularly in alloys. The maps are only as good as the constitutive equations—be they theoretical or empirical—used to construct them. Yet for comparison purposes, many of these criticisms do not apply. If we simply wish to compare different f.c.c. metals, or compare typical f.c.c. with typical b.c.c. metals as we do in the next section, then (since the same assumptions were used to construct all maps) the comparison is a valid one.

4. APPLICATION OF THE MAPS

4.1 *Effect of bond-type and crystal structure on plastic properties*

Suppose one could produce metals, non-metals, oxides and other materials with the same microstructural features. Then the difference in their strengths would have its origin in their crystallography and the nature of the bonds holding their atoms together. The next sequence of maps shows the results of such an investigation. To make the comparison easier, the maps show only one strain-rate contour: that for $\dot{\varepsilon} = 10^{-8}$/sec. All maps refer to a standard microstructural state: a grain size of 32 μ, and an obstacle density of 4×10^{10}/cm^2. The comments below refer to this standard state.

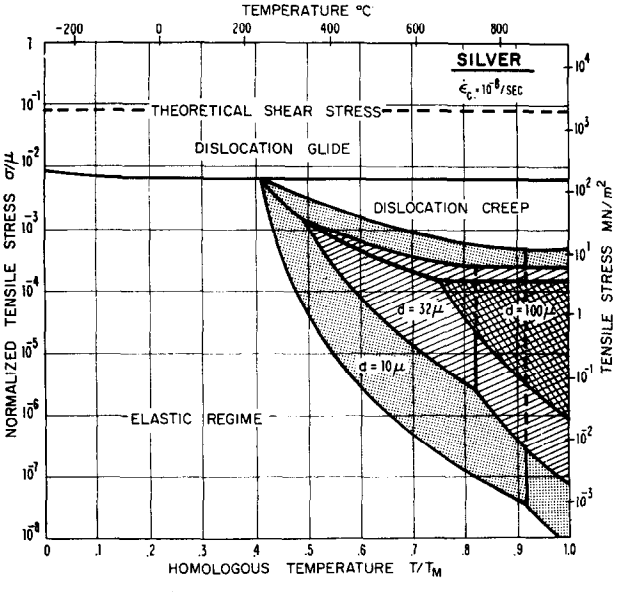

FIG. 6. Changing the grain size d, expands or contracts the diffusional-flow fields. It also has a small effect on the dislocation glide field (not shown).

In all, I investigated 7 f.c.c. metals; maps for three of them are shown in Fig. 7, and a fourth was shown as Fig. 1. All have well developed Nabarro and Coble creep fields. Silver (Fig. 1) typifies the noble metals Cu, Ag, Au. For all three the temperature separating the Nabarro-creep from Coble-creep occurs between $0.8T_M$ and $0.9T_M$.

The other f.c.c. metals (lead, aluminum, nickel and gamma-iron) are somewhat more varied. All have higher values for the transition temperature. Aluminum has a particularly large dislocation-creep field. Nickel appears to be particularly sensitive to Coble

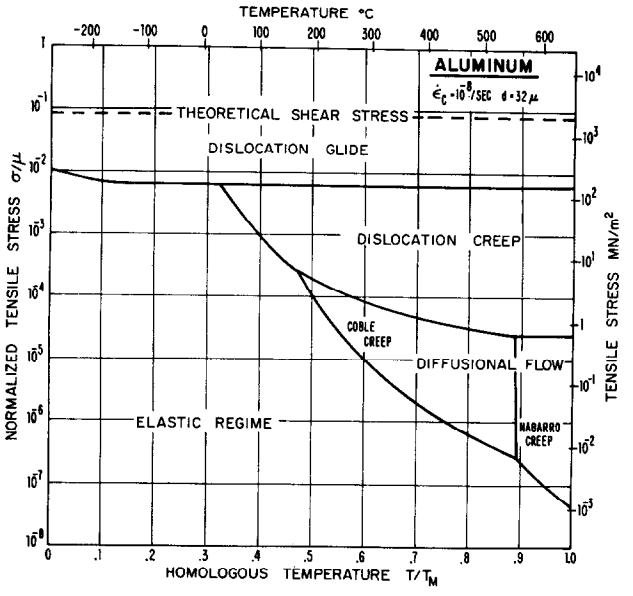

(a)

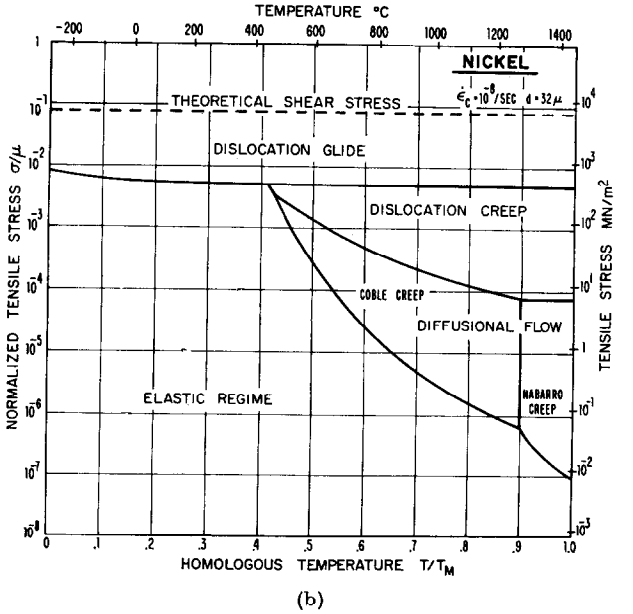

(b)

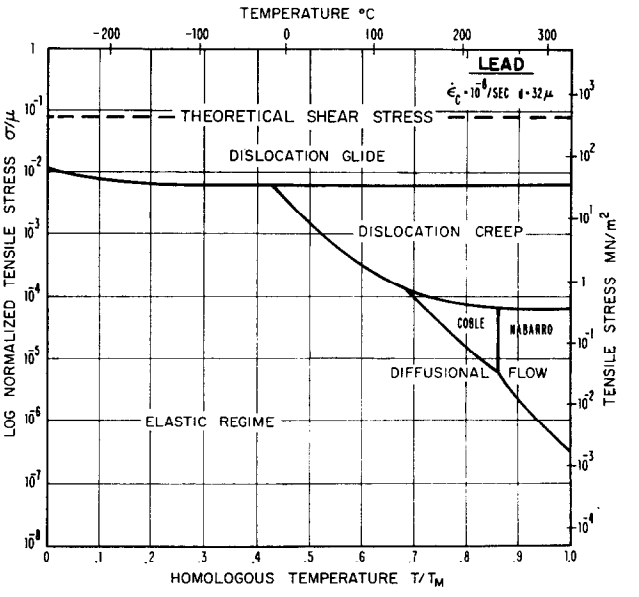

(c)

FIG. 7.(a)–(c) Specialized maps for $\dot{\varepsilon}_c = 10^{-8}$/sec, $d = 32\ \mu$ and $\rho = 4 \times 10^{10}$/cm² for three f.c.c. metals: (a) nickel, (b) aluminum, (c) lead. A similar map for silver was shown in Fig. 1.

creep. Lead has exceptionally small diffusional flow fields, reflecting its relatively small diffusion coefficients. All in all, however, the f.c.c. metals fall into a broad class, with remarkably similar maps. This is true not only of the specialized maps in Fig. 7, but of the complete maps such as Fig. 3. The small differences between them stem mainly from the differences in diffusion coefficients (among f.c.c. metals, diffusion coefficients normalized to the melting point vary by a factor of about 20).

Figure 8 shows maps for hexagonal metals. Those with non-ideal c/a ratios—cadmium and zinc, for instance—appear to differ from f.c.c. metals, being more susceptible to Nabarro creep. This enlarges the Nabarro-creep field at the expense of that for Coble creep, pushing the transition temperature which separates them to lower temperatures. Although the data used to construct the maps is really not accurate enough to be sure of this conclusion, the one hexagonal metal with an almost ideal c/a ratio (thallium) does not show this extended diffusional-creep field.

The maps for b.c.c. metals do differ in a significant way from those for h.c.p. and f.c.c. metals. Five were investigated; maps for two are shown in Fig. 9. The bulk diffusion coefficients of b.c.c. metals are significantly larger, at a given homologous temperature than those of the close packed metals. This swells the Nabarro and the dislocation creep fields at the expense of the Coble creep field, which (for this standard

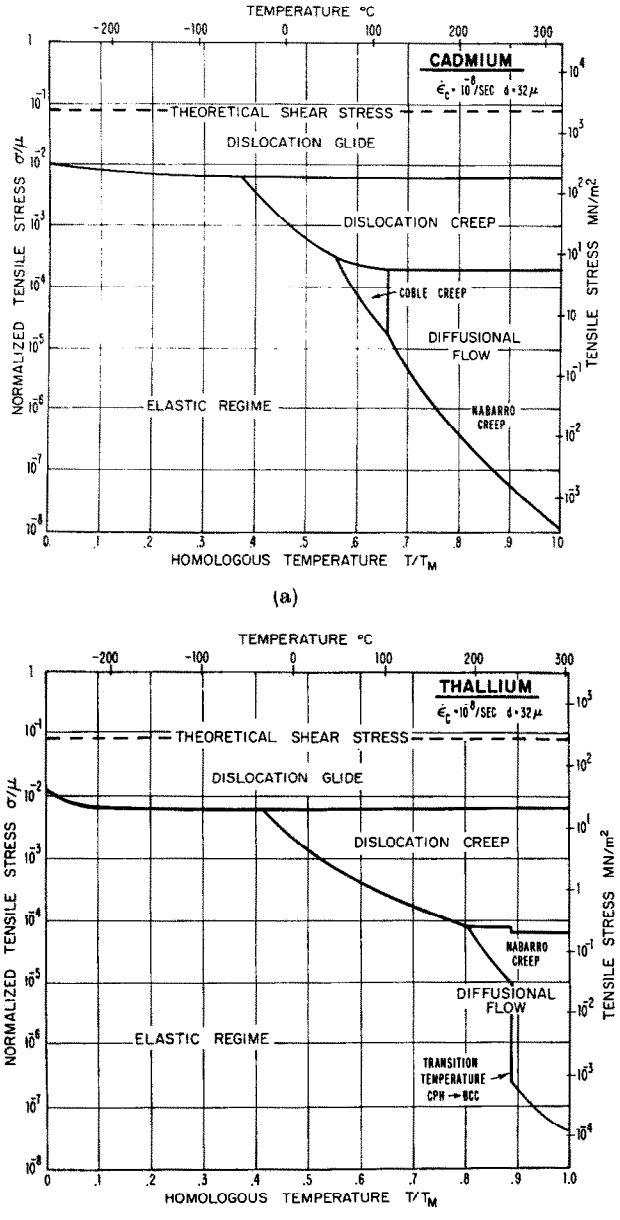

FIG. 8. Specialized maps for two hexagonal metals: (a) cadmium and (b) thallium. Thallium transforms to a b.c.c. structure at 230°C, when its creep rate increases because diffusional transport through it is faster.

set of conditions) almost disappears. This is because, although the relative rate of *bulk* diffusion is larger in b.c.c. metals, that of *boundary* diffusion apparently is not. The low-temperature strength of b.c.c. metals is more strongly temperature dependent than that of close packed metals because of the lattice resistance [equation (2b)]. Like those for f.c.c. metals, the b.c.c. maps form a group with broadly similar characteristics.

The effect of a phase change on creep is illustrated by the maps for thallium [Fig. 8(b)] and for iron [Fig. 9(b)]. They help to emphasize the fact that the close-packed structure is intrinsically more creep-resistant than the b.c.c. structure.

The diamond-cubic elements Ge and Si show extremely small diffusional-creep fields (Fig. 10). This is a direct result of the large energy-of-formation of a vacancy (and consequent low rate of diffusive transport) which is characteristic of this structure. A direct comparison between silver and germanium is a

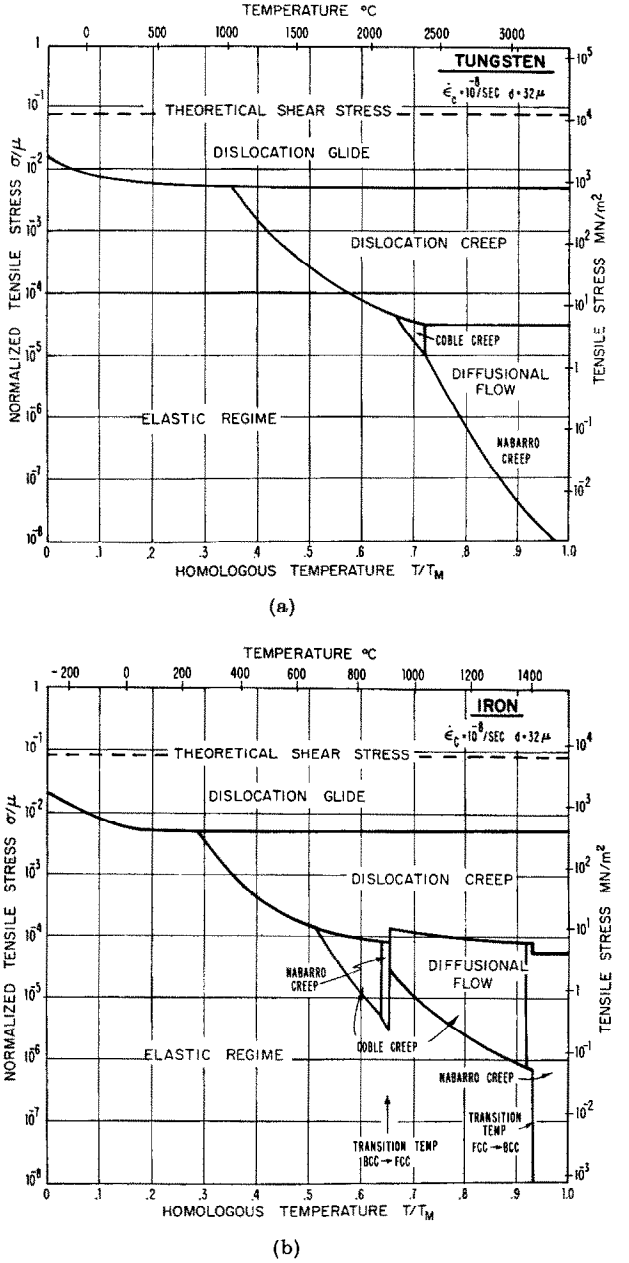

FIG. 9. Specialized maps for b.c.c. metals: (a) tungsten; (b) iron. Iron transforms to an f.c.c. structure at 911°C and back to a b.c.c. structure at 1392°C. Note that the f.c.c. form of iron creeps less fast than the b.c.c. form because of its relatively smaller diffusion coefficients.

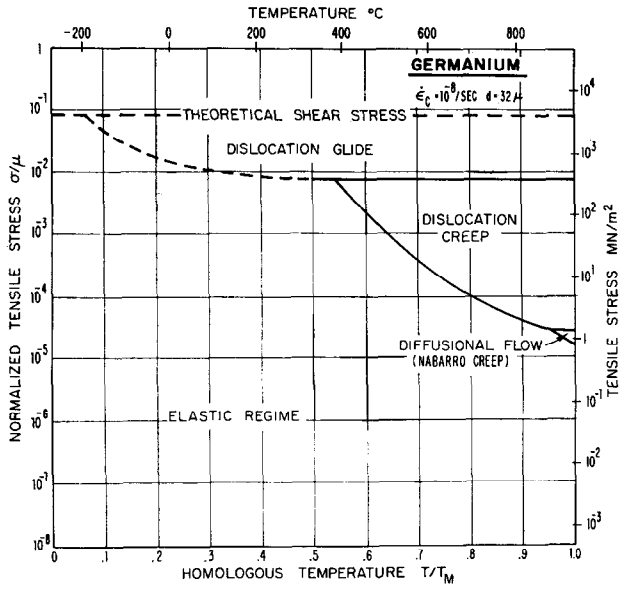

FIG. 10. A specialized map for germanium.

profitable one, since the two in almost all other respects are very similar (in melting point, shear modulus, cohesive energy).

Oxides (Fig. 11) are much more variable—and the data for them is much less reliable—than metals. They show smaller diffusional-creep fields than metals, and for the standard set of conditions, the Coble creep field is absent. (Remember, however, that for some other set of conditions, it would re-appear.) Any attempt to plot reliable maps for oxides is frustrated at present by the lack of reliable diffusion data.

4.2 *Design and interpretation of experiments; and the search for missing mechanisms*

By far the most useful form of the maps is that shown in Figs. 3 and 4. A set of such maps, spanning the normal range of grain sizes (say 1 μ to 1 mm) summarizes the entire state of our knowledge of steady-state flow for a given material. If one wishes to design an experiment to study Coble creep, for instance, then the appropriate map shows the range of stress and temperature which should be applied to specimens in order that they deform by Coble creep; it further indicates the strain-rate to be expected. More accurately, it shows the best guess that our present knowledge of plastic flow allows us to make.

The maps are based on our current understanding of creep and plastic flow mechanisms, and on experimental data. In spite of the long history of mechanical metallurgy, neither is complete or wholly trustworthy. It has become clear from a survey of the literature, and from our work, that *mechanisms are missing* from the maps shown here: at low temperatures ($<\frac{1}{2}T_M$) for instance, it is clear that a non-linear creep field separates the glide field from the Coble-creep field. There is evidence that the constitutive equation for diffusional flow may be incorrect, predicting strain-rates that are a factor of 10 too small, perhaps because of another missing mechanism. Further, at certain of the boundaries between two fields, complicated *combined mechanisms* occur (for instance, grain-boundary sliding coupled with dislocation creep) which are not simply the linear superposition of the two mechanisms which meet at the boundary. It is tempting to

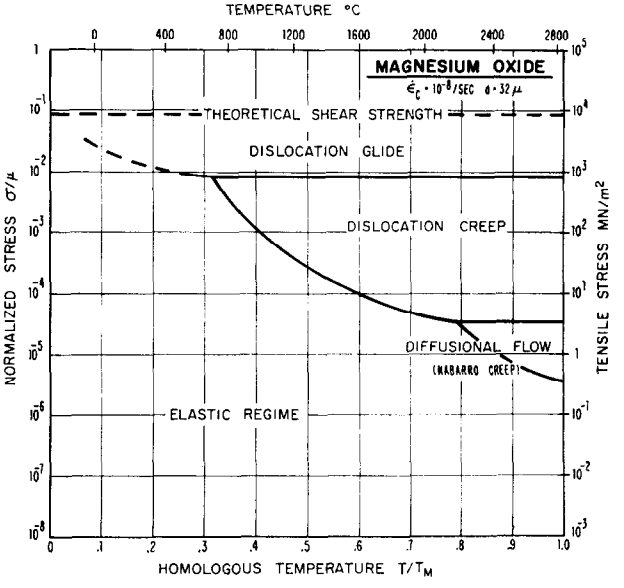

(a)

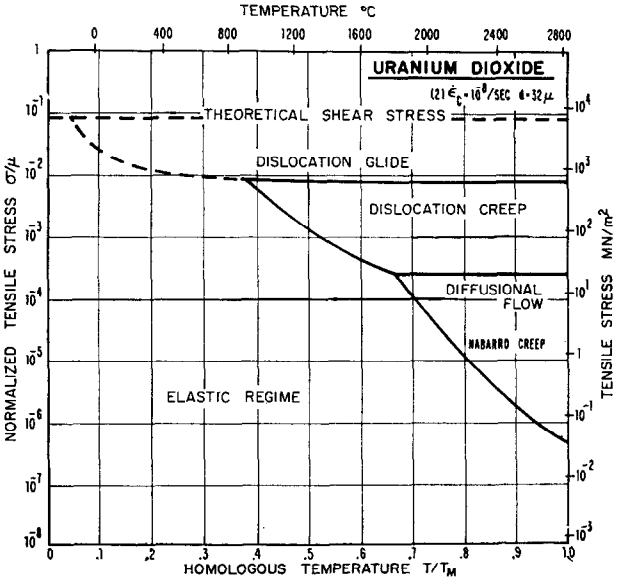

(b)

FIG. 11. Specialized maps for oxides: (a) magnesium oxide; (b) stoichiometric uranium dioxide.

ask whether *superplastic flow* is an independent deformation mechanism and should therefore appear as a field in its own right. At present these missing mechanisms are too poorly understood to include them; but the maps help localize the regime of stress, temperature, strain-rate and grain size for which data (and a theoretical understanding) are needed.

Finally they help in obtaining reliable constitutive equations from experiments. If experiments are conducted well within a field, *where a single mechanism is dominant*, then the results can be used to construct a constitutive equation which can legitimately be used to extrapolate the effects of that mechanism to other temperatures or stresses. But data obtained at or near a field boundary must not be used in this way: on changing the stress or temperature the relative contributions of the two mechanisms which meet at the boundary change also. No single constitutive equation can describe the results; extrapolation is dangerous.

4.3 *Engineering applications and useful strengthening mechanisms*

Suppose—to take an example—that a turbine blade operates with a known temperature and stress distribution on it. This *stress–temperature profile* can be plotted onto the map (like those of Figs. 3 and 4) appropriate to the material, as a line or band. The mechanism by which each part of the blade deforms, the strain-rate of that part and the appropriate constitutive equation, can be read immediately from the map. Problems involving multiaxial stress states are handled by computing equivalent stresses (and strain-rates) via the von Mises (or equivalent) equation.

A strengthening mechanism is only *useful* if it slows the rate of deformation in the right field of the map. A mechanism—dispersion hardening for example—which slows dislocation creep has further repercussions: it results in the movement of field boundaries such that the dislocation-creep field shrinks and the diffusional fields expand. To continue the example of the last paragraph: a turbine blade that previously lay in the dislocation creep field may now deform by another mechanism—diffusional creep. Further inhibition of dislocation creep is useless; the blade now deforms by diffusional creep, which (in general) is not susceptible to the same strengthening mechanisms which work for dislocation creep.

5. SUMMARY AND CONCLUSIONS

1. Sufficient theory and data exist to permit the construction of *deformation–mechanism maps* showing the fields of stress and temperature in which each of six (or more) independent mechanisms for plastic flow is dominant. Knowledge of any two of the three variables of stress, temperature and strain-rate locates a point on the map, identifies the dominant mechanism or mechanisms and gives the value of the third variable.

2. Like phase diagrams, the maps are only as good as the theory and the experimental data used to construct them—and at the present both must be termed poor. But—like phase diagrams—they are useful in spite of their inexactness for both designing and interpreting experiments and in selecting and understanding the behavior of materials for engineering applications. And, by identifying the places where data or theory are poor, they can be systematically improved.

ACKNOWLEDGEMENTS

This work was supported in part by the Advanced Research Projects Agency under Contract DAHC15-67-C-0219, in part by the Office of Naval Research under Contract N00014-67-A-0298-0020 and by the Division of Engineering and Applied Physics, Harvard University.

REFERENCES

1. A. Kelly, *Strong Solids*. Oxford University Press (1966).
2. A. G. Evans and R. D. Rawlings, *Phys. Status Solidi* **34,** 9 (1969).
3. U. F. Kocks, A. Argon and M. F. Ashby, *Proc. Metal. Phys.* to appear.
4. P. Guyot and J. E. Dorn, *Can. J. Phys.* **45,** 983 (1967).
5. R. Raj and M. F. Ashby, *Trans. metall. Soc. A.I.M.E.* **2,** 1113 (1954).
6. A. K. Mukherjee, J. E. Bird and J. E. Dorn, *Trans. Am. Soc. Metals* **62,** 155 (1969).
7. J. Weertman, *Trans. metall. Soc. A.I.M.E.* **227,** 1475 (1963).
8. F. A. McClintock and A. Argon, *Mechanical Behavior of Materials*, chapter 7. Addison Wesley (1966).
9. N. L. Peterson, *Solid St. Phys.* **22,** (1968).
10. J. R. Neighbors and G. A. Alers, *Phys. Rev.* **111,** 707 (1958).
11. R. E. Hoffman and D. Turnbull, *J. appl. Phys.* **22,** 634 (1951).
12. W. C. Overton and J. Gaffney, *Phys. Rev.* **98,** 969 (1955).
13. Y. A. Chang and L. Himmel, *J. appl. Phys.* **37,** 3567 (1966).
14. H. B. Huntington, *Solid St. Phys.* **7,** 213 (1958).
15. A. R. Wazzan, *J. appl. Phys.* **36,** 3596 (1965).
16. W. Koster, *Z. Metalk.* **39,** 1 (1948).
17. B. Okkerse, T. J. Tiedema and W. G. Burgers, *Acta Met.* **3,** 300 (1955).
18. D. W. James and G. M. Leak, *Phil. Mag.* **12,** 491 (1965).
19. E. S. Wadja, G. A. Shirn and H. B. Huntington, *Acta Met.* **3,** 39 (1955).
20. E. S. Wadja, *Acta Met.* **2,** 184 (1954).
21. P. E. Armstrong and H. L. Brown, *Trans. metall. Soc. A.I.M.E.* **230,** 962 (1964).
22. Data of R. L. Andelin, J. D. Knight and M. Kahn, *Trans. metall. Soc. AIME.* **233,** 19 (1965) as modified by S. L. Robinson and O. D. Sherby, *Acta Met.* **17,** 109 (1969).
23. K. G. Kreider and G. Bruggeman, *Trans. metall. Soc. AIME.* **239,** 1222 (1967).

TABLE 1

Data for pure metals and oxides	Atomic volume $\Omega \times 10^{23}$ (cm)	Burger's vector $b \times 10^{8}$ (cm)	Melting temperature T_M (°K)	Shear modulus at 300°K $\mu \times 10^{-11}$ (dyn/cm²)	T-dependence of shear modulus $\frac{1}{\mu}\frac{d\mu}{dt} \times 10^{4}$ (/°K)	D_0 for bulk diffusion $(D_0)_{vol}$ (cm²/sec)	Activation energy for bulk diffusion Q_{vol} kcal/mole	D_0 for boundary diffusion $(D_0)_{bdry}$ (cm²/sec)	Activation energy for boundary diffusion Q_{bdry} (kcal/mole)	Dimensionless constant of equation (5) A	Dimensionless exponent of equation (5) n
Silver	1,71	2.89	1234	2.64[10,13]	4.36[10,13]	0.44[9]	44.3[9]	0.09[11]	21.5[11]	2.30×10^{6}	5.3[6]
Copper	1.18	2.56	1356	4.21[12,13]	3.97[12,13]	0.62[9]	49.6[9]	0.1*	24.8*	7.40×10^{5}	4.8[6]
Gold	1.70	2.88	1336	2.48[10,13]	3.18[10,13]	0.091[9]	41.7[9]	0.1*	20.8*	5.75×10^{8}	5.5[6]
Nickel	1.09	2.49	1726	7.87[14]	3.7[14]	1.9[9]	68.0[9]	0.07[15]	27.4[15]	3.83×10^{5}	4.6[6]
Aluminum	1.66	2.86	933	2.54[14]	5.4[14]	0.035[9]	28.8[9]	0.1*	14.4*	3.40×10^{6}	4.4[6]
Lead	3.03	3.5	600	0.534[14]	14.4†[14]	1.37[9]	26.1[9]	1.6[17]	15.7[17]	3.78×10^{4}	4.2[6]
γ-iron	1.21	2.58	1809	8.1†	5.35†	0.18[9]	64.5[9]	1.5[18]	38.0[18]	4.10×10^{10}	5.75[6]
Cadmium	2.16	2.98	594	2.8†	9.4†	0.05‡	18.2‡	1.0[19]	13.0[19]	1.70×10^{3}	4.3[6]
Zinc	1.52	2.67	693	3.6†	8.0†	0.13‡	21.9‡	0.26[20]	14.45[20]	1.47×10^{10}	6.1[6]
α-thallium	2.86	3.46	576	0.3†	7.0†	0.4‡	22.9‡	1.0*	15.6*	3.66×10^{8}	5.3[6]
Molybdenum	1.56	2.73	2883	12.5[14]	1.42†	0.1[9]	92.2[9]	1.0*	62.8*	4.02×10^{4}	4.3[6]
Tantalum	1.80	2.86	3253	7.05†	1.3†	0.12[9]	98.7[9]	1.0*	67.0*	7.55×10^{5}	4.2[6]
Tungsten	1.59	2.74	3683	15.5[14]	1.04[21]	5.6[22]	140.0[22]	10.0[23]	90.5[23]	1.99×10^{12}	5.8[6]
β-thallium	2.92	3.36	576	0.55†	17.0†	0.7[9]	20.0[9]	1.0*	13.6*	1.45×10^{11}	5.8[6]
α-iron	1.18	2.48	1809	8.1†	3.3†	2.0	57.3[9]	1.2[24]	33.4[24]	7.33×10^{14}	6.9[6]
δ-iron	1.25	2.54	1809	8.1†	3.3†	1.9[9]	57.0[9]	1.2[24]	33.4[24]	7.33×10^{14}	6.9*
Germanium	2.26	3.99	1210	5.2[25]	0.0	87.0[26]	73.5[26]	87.0[26]	53.0[26]	1.28×10^{6}	4.2§
MgO	1.87	4.2	3125	13.0[27]	2.62[27]	2.5×10^{-6}	62.4[28]	2.5×10^{-6}*	41.2*	11.6	3.3[37]
Stoichiometric UO_2	4.08	3.865	3123	8.3[29]	1.0[29]	4.3×10^{-4}[30]	88.0[30]	4.0×10^{-2}[31]	70.0[31]	5.5×10^{3}	4.5[34]

* Inferred by scaling data of materials of the same structure and comparable melting point.
† Approximated as $\mu = E/2(1+\nu)$ assuming $\nu = \frac{1}{3}$ and with the same temperature dependence as Young's modulus, E, using data of Koster.[16]
‡ Data for diffusion parallel to the c-axis, from Ref. 9.
§ Inferred from data of Alexander.[32] Data must be regarded as unreliable and probably not referring to a steady state.

24. V. T. Borisov, V. M. Golikov and Scherbedinskiy, *Fizika Metall.* **17,** 80 (1964).
25. W. L. Bond, W. P. Mason, H. J. McSkimin, K. M. Olsen and G. K. Teal, *Phys. Rev.* **80,** 176 (1950); H. J. McSkimin, W. L. Bond, E. Buehler and G. K. Teal, *Phys. Rev.* **83,** 1080 (1951).
26. H. Letaw, L. M. Slifkin and W. M. Portnoy, *Phys. Rev.* **93,** 892 (1954).
27. H. Spetzler, *J. Geophys. Res.* **75,** 2073 (1970).
28. I. Oishi and W. Kingery, *J. chem. Phys.* **33,** 905 (1960).
29. J. B. Wachtman Jr., M. L. Wheat, H. J. Anderson and J. L. Bates, *J. Nuclear Mater.* **16,** 39 (1965); P. Sung and J. E. Turnbaugh, *J. Nuclear Mater.* **24,** 107 (1967).
30. A. B. Auskern and J. Belle, *J. Nuclear Mater.* **33,** 311 (1961).
31. A. B. Alcock, R. J. Hawkins, A. W. D. Hills and P. McNamara, *Thermodynamics*, p. 57. I.A.E.A. (1966).
32. H. Alexander and P. Haasen, *Solid St. Phys.* **22,** 141 (1968).
33. T. A. Langdon and J. A. Pask, *Acta Met.* **18,** 505 (1970).
34. J. A. Roberts, private communications.

APPENDIX

Details of the computation

The *field boundaries* were computed by equating the constitutive equations (1)–(5) in pairs, and solving the resulting implicit equation for stress as a function of temperature. The *contours of constant strain rate* were obtained directly from the constitutive equation *for that field*; this ignores contributions from the mechanisms from neighboring fields which, strictly, should be added to major contribution of the dominant mechanism.

Wherever possible the shear modulus was calculated as

$$\mu = \sqrt{\tfrac{1}{2}c_{44}(c_{11} - c_{12})}$$

I aimed at accuracy to within a factor of 2. Since the shear modulus can vary by this factor between 0°K and the melting point, a linear temperature dependence of the modulus was included. The atomic volume, on the other hand, varies much less rapidly with temperature; this dependence was ignored.

The input data for the calculations, and its source, is listed in Table 1. Diffusion data for non-metals, much of the grain boundary diffusion data, and much dislocation creep data cannot be regarded as accurate to within a factor of 2. In certain cases, data were not available for boundary diffusion coefficients, or for the Peierls potential. In these cases, rather than leave out fields which certainly must exist, data were *inferred* by scaling data for other materials of the same structure and of similar melting point. Such data are referred to as "inferred data" (*) in Table 1.

The theoretical shear strength was taken to be 0.039 μ. Strictly, it is structure dependent (Kelly[1]) but for our purposes, a single, constant value for all materials is adequate.

The effect of a Peierls potential was included for b.c.c. metals. The necessary data is shown in Table 2

Table 2

	Peierls stress $\tau_p \times 10^9$ (dyn/cm²)	Activation energy for kink nucleation $u_k \times 10^{12}$ (eV)	Preexponential factor $\dot{\gamma}_0'$ (/sec)	References
Molybdenum	4.13	0.62	10^4	4
Tantalum	3.34	0.31	10^4	4
Tungsten	4.1	0.6	10^4	*
α-iron	4.5	0.31	10^4	4

* No data available. Data for molybdenum used for tungsten calculation.

and refers to shear stress and shear strain rate; conversion to tensile stress and strain rate simply requires setting $\sigma_p = \sqrt{3}\tau_p$ and $\sqrt{3}\dot{\varepsilon}_0' = \dot{\gamma}_0'$. The quantity $\dot{\gamma}_0'$ was chosen so that the contribution of the Peierls resistance to the flow stress becomes negligible above a characteristic temperature. By fitting the equation to data for tantalum, the value $\dot{\gamma}_0' = 10^4$ was obtained.

As pointed out in the text, a standard *microstructural state* must be chosen to make maps for different materials comparable. The "specialized maps" of Figs. 7–11 were computed for an obstacle spacing of $\frac{1}{2} \times 10^{-5}$ cm and a grain size of 32×10^{-4} cm.